ELSEVIER

Journal of Molecular Catalysis A: Chemical 149 (1999) 205–213

JOURNAL OF MOLECULAR CATALYSIS A: CHEMICAL

www.elsevier.com/locate/molcata

Structure, acidity and catalytic properties of dealuminated SAPO-11 molecular sieves

Huiping Tian [a,*], Chenglie Li [b]

[a] *Division 14, Research Institute of Petroleum Processing, 18 Xueyuan Road, P.O. Box 914-14, Beijing 100083, China*
[b] *Petroleum Processing Research Center, East China University of Science and Technology, 130 Meilong Road, Shanghai 200237, China*

Received 8 July 1998; accepted 1 March 1999

Abstract

A SAPO-11 molecular sieve was dealuminated in H_4EDTA solution to different Al content. Dealuminated samples were characterized by catalytic transformation of butene, *o*-xylene and cumene, IR analysis of adsorbed pyridine and ^{31}P-, ^{29}Si-MAS-NMR. Dealumination resulted in formation of strong Bronsted acid sites around Si domains. Amorphous $AlPO_4$ formed by deep dealumination of SAPO-11, led to a decrease of Bronsted acidity. The Lewis acidity was reduced by dealumination. The acidity of dealuminated SAPO-11 was measured and used to elucidate the catalytic properties. Butene isomerization was proceeded on Bronsted acid sites of medium strength. The selectivity of toluene disproportionation was favored on Lewis acid sites by low temperature and space velocity. Dealumination of SAPO-11 samples improved cumene cracking, especially at high temperatures. The reaction kinetics and mechanism were discussed.

Keywords: Dealuminated SAPO-11; Acidity; Butene isomerization; Toluene disproportionation; Cumene cracking

1. Introduction

Based on the fact that SAPO-11 can effectively convert linear olefins into branched olefins [1,2], which face an increasing commercial requirements, such as *iso*-butene to the need of MTBE (methyl tertiary butyl ether) production, studies of SAPO-11 are growing rapidly [3,4]. Furthermore, the unique acidity of SAPO-11 has evoked a widespread catalytic applications, for example, phenol butylation [5] and biphenyl alkylation [6].

The formation and modification of SAPOs are possible by means of hydrothermal method [7]. SAPO-11 has been hydrothermally synthesized with *n*-Pr_2NH-TPAOH (*n*-di-propyl amine and tetrapropylammonium hydroxide) or *iso*-Pr_2NH-propanol mixtures as template [8], but the modification of SAPO-11 is to be explored.

In this paper, SAPO-11 was synthesized with *iso*-Pr_2NH as a novel organic template, and dealuminated in H_4EDTA (ethylene di-amine tetraacetic acid) solution. Dealumination and its influence on surface acidity and catalytic behavior in linear butene skeletal isomerization, toluene disproportionation and cumene cracking were discussed.

* Corresponding author

1381-1169/99/$ - see front matter
PII: S1381-1169(99)00176-4

2. Experimental

2.1. SAPO-11 samples

SAPO-11 was synthesized by hydrothermally crystallizing a sol–gel mixture with a composition of SiO_2:P_2O_5:Al_2O_3:H_2O:*iso*-Pr_2NH = (0–0.5):1.2:1.0:55:1.1 in an autoclave at 453 K for 48 h. Dealumination of SAPO-11 was achieved in a 0.01–0.08 M H_4EDTA solution at 338 K. Crystalline products of synthesis and dealumination process were recovered by washing and filtering, then dried at 393 K for 5 h and calcined at 773 K for 1 h.

2.2. Characterization

X-ray diffraction (XRD) measurement was conducted on a diffractometer D/max-gamma B using Cu K-alpha radiation. Chemical composition of crystalline products was determined with a Hitachi 180-80 spectrometer. ^{31}P, ^{29}Si MAS-NMR (magic angle spinning nuclear magnetic resonance) spectra were taken on a Varian VXR-200s spectrometer with a Doty Scientific CP-MAS probe.

Infrared (IR) spectra of adsorbed pyridine on SAPO-11 were recorded on a 20SX FT spectrometer at 10^{-7} Pa. SAPO-11 samples were initially activated in vacuum at 773 K for 2 h, then reduced to room temperature, followed by contacting with pyridine vapor. After that, temperature was stepwise increased for measurement.

Catalytic evaluation was performed in a microreactor-GC (gas chromatography) system loaded with 1.0–1.5 g SAPO-11 samples under normal pressure. Skeletal isomerization of linear butenes was conducted at 573–823 K. Hydrocarbon feed contains linear butenes 68.0 wt.%, *iso*-butene 0.50 wt.%, butane 31.20 wt.%, C_5 and heavier 0.04 wt.%, C_1–C_3 0.26 wt.%. Toluene agent (CP grade) was diluted by H_2 to 23.3 wt.% and used in catalytic disproportionation evaluation which was conducted at 753–803 K. Cumene cracking was carried out at 653–703 K with 21.6 wt.% of cumene in H_2 as reactant. The feed rate in the evaluation was controlled to keep a WHSV of linear butenes, toluene or cumene of 1.0 h^{-1}. The coke content after 0.5 h reaction was determined by O_2 consumption at 873 K.

3. Results and discussion

3.1. Structure and acidity of dealuminated SAPO-11

The synthesis of SAPO-11 with *iso*-Pr_2NH as a novel template was verified by XRD measurement [9]. Table 1 lists compositions of SAPO-11 and its dealuminated derivatives. In $AlPO_4$-11 molecular sieve, Al and P was alternately distributed. When Si was introduced into $AlPO_4$-11, it preferably took the same position as P in framework [10]. The molar content of Si and P in framework was exactly 0.50 for No. 1 SAPO-11 sample having low Si level. This implied the equivalent substitution of P by Si. No. 2 SAPO-11 sample contained Si to a level that Si and P molar content in framework was

Table 1
Molar compositions of SAPO-11 and its dealuminated derivatives

No.	Chemical composition ($aSiO_2 \cdot bAl_2O_3 \cdot cP_2O_5$)			Framework composition ($Si_xAl_yP_z$)O_2		
	a	*b*	*c*	*x*	*y*	*z*
1	1.0	5.0	4.5	0.05	0.50	0.45
2	1.0	3.1	2.7	0.08	0.49	0.43
1-L1[a]	1.0	4.8	4.5	0.05	0.48	0.45
1-L2[b]	1.0	4.7	4.4	0.05	0.45	0.43

[a] No. 1 sample after slight dealumination.
[b] No. 1 sample after deep dealumination.

more than 0.50. As a result, it was quite probable that Si domains formed in No. 2 sample. This was confirmed by ^{29}Si MAS-NMR analysis as shown in Fig. 1 (curve (*b*)). Peak at −110 ppm represented the Si(4Si) environment [11], indicating the existence of Si domains. Peak at −89 ppm was probably to be Si(4Al) environment. Peaks between −110 and −89 ppm might stand for Si having (1–3)Al atoms as adjacent neighbors.

No. 1 SAPO-11 sample was dealuminated to two Al levels as listed in Table 1. ^{29}Si MAS-NMR spectra of the dealuminated SAPO-11 is shown in Fig. 1 (curve (*a*-L1) and (*a*-L2)). Since the −110 ppm peak stands for Si domains (Si(4Si)) [11], slight dealumination might lead to the formation of Si domain as the case of No. 1-L1 sample (Fig. 1, curve (*a*-L1)). This was an evidence of ease removal of Al located between or among Si atoms in framework. The chemical composition was not equivalent to the framework composition of No. 1-L2 sample, that implied the formation of amorphous phase in the case of deep dealumination. Furthermore, on ^{31}P MAS-NMR spectrum of deep-

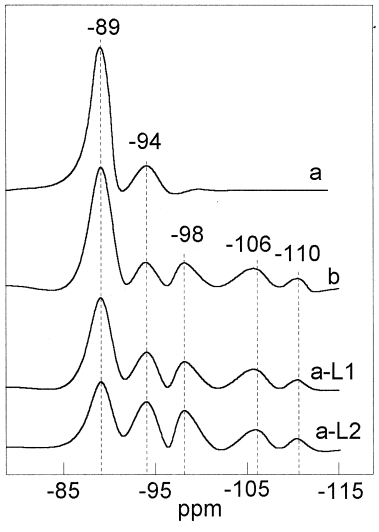

Fig. 1. ^{29}Si MAS-NMR spectra of No. 1 SAPO-11 sample (curve (*a*)), No. 2 SAPO-11 sample (curve (*b*)), No. 1-L1 SAPO-11 sample (curve (*a*-L1)) and No. 1-L2 SAPO-11 sample (curve (*a*-L2)) in Table 1.

dealuminated SAPO-11 sample, a new band peak at −20 to −23 ppm was observed. This peak was assigned to amorphous $AlPO_4$ phase [12], This suggested that Al in P environment was removed only in deep dealumination stage, and its removal resulted in a loss of crystallinity. Based on the structure of SAPOs [13,14], dealumination process and structure of dealuminated SAPO-11 can be illustrated in Fig. 2.

IR spectra of adsorbed pyridine were applied to detect the number of acidic sites of SAPO-11 samples. The band at 1550 cm^{-1} attributed to cation chain stretching of pyridine ions and exhibited Bronsted acidity, and the 1455 cm^{-1} band was assigned to carbon chain stretching of coordinately bonded pyridine complexes and indicating the presence of Lewis acidity [15–17]. Fig. 3 shows the change of 1455 and 1550 cm^{-1} band intensities of SAPO-11 at different temperatures. Pyridine desorbed from Bronsted sites more easier than from Lewis sites with temperature increase, especially above 673 K. This indicated that Bronsted acidity mainly remained in intermediate range below 673 K, and its strength is lower than that of Lewis acidity. After slight dealumination (No. 1-L1), the amount of Lewis acidity below 673 K decreased, while the acidity at 773 K kept stable. After deep dealumination (No. 1-L2), Lewis acidity was decreased in whole temperature range. Dealumination brought a different effect on Bronsted acidity from that on Lewis acidity. The amount of Bronsted acidity below 673 K reduced with dealumination, while the amount of Bronsted acidity at 773 K increased with dealumination. This meant that Bronsted acidity was uniformly distributed in whole temperature range upon dealumination. Taking into account the structure and composition changes, it was believed that the formation of Si domain enhanced the amount of Bronsted acidity at 773 K and restrained the intermediate Bronsted acidity below 673 K.

When No. 1-L1 sample was pretreated with steam, the amount of pyridine on Bronsted sites

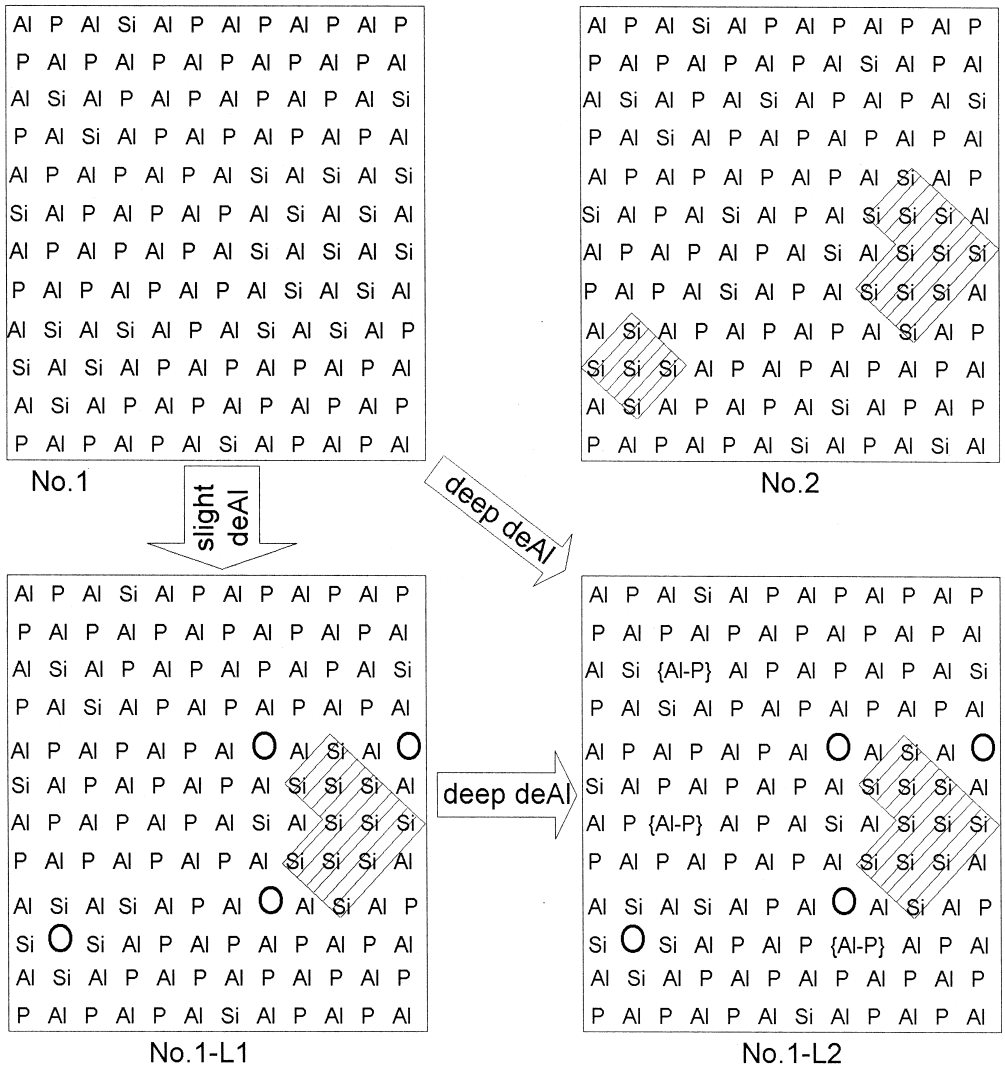

Fig. 2. Planar scheme for the arrangement of Si, Al, P in framework of SAPO-11 and dealuminated derivatives. {Al–P} stands for amorphous phase, ○ stands for vacancy after dealumination. Shadow stands for Si domain.

and Lewis sites varied in a great deal (Fig. 3). The amount of Bronsted acidity increased below 673 K, unchanged at 773 K. The amount of Lewis acidity decreased, probably due to the conversion of Lewis sites to Bronsted sites by H_2O chemisorption.

3.2. Butene catalytic skeletal isomerization

The product distribution of catalytic skeletal isomerization of linear butenes is exemplified in Table 2. The following reactions were inferred to be included in the process: isomerization of linear butenes, hydrogenation of olefins, oligomerization of olefins, and cracking of hydrocarbons. Furthermore, all of these reactions but isomerization were accelerated by increasing temperature. This was explained by means of thermodynamic equilibrium [18].

Fig. 4 shows temperature dependence of coke yield, linear butene conversion and *iso*-butene selectivity. Linear butene conversion was de-

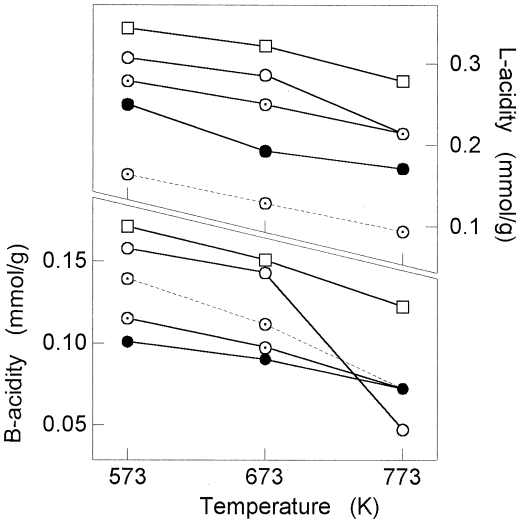

Fig. 3. Temperature dependence of the amount of pyridine on Bronsted sites and Lewis sites of SAPO-11 samples (○) No. 1, (□) No. 2, (⊙) No. 1-L1, and (●) No. 1-L2 in Table 1. Dashed line stood for the experiment in which sample (No. 1-L1) had been pretreated in steam at 773 K for 0.5 h.

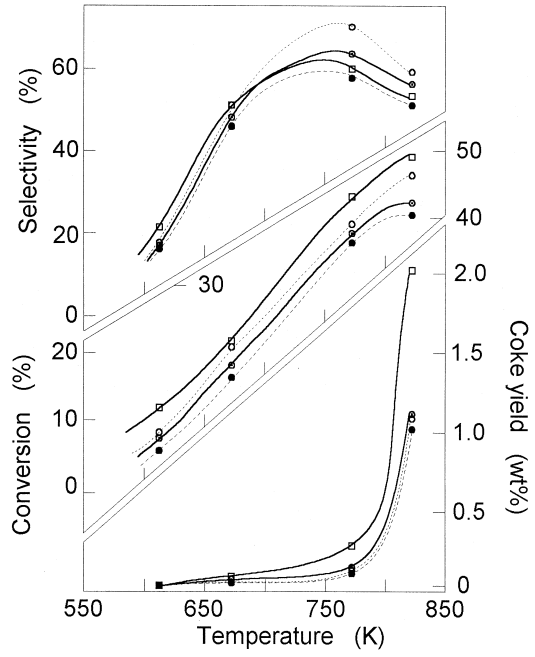

Fig. 4. Temperature dependence of conversion, selectivity and coke yield in butene isomerization evaluation over No. 1 SAPO-11 sample (· · · ○), No. 2 SAPO-11 sample (——— □), No. 1-L1 SAPO-11 sample (———⊙) and No. 1-L2 SAPO-11 sample (---●) in Table 1.

fined as (decrease of weight percentage of linear butenes after reaction)/(weight percentage of linear butenes in feed), and *iso*-butene selectivity was defined as (increase of weight percentage of *iso*-butene after reaction)/(decrease of weight percentage of linear butenes after reaction). *iso*-Butene selectivity varied in a volcano fashion with temperature, and the maximum selectivity was achieved at 673 K. Coking phenomenon became serious at 673 K and higher temperatures that was consistent to the selectivity drop, while the conversion linearly increased. No. 1 sample had a preferred *iso*-butene selectivity, and No. 2 sample that was rich in Si showed high linear butene conversion. Dealumination inhibited both linear butene conversion and *iso*-butene selectivity. Compared with No. 1 sample, increase of Si content (No. 2 sample) or slight dealumination (No. 1-L1 sample) caused a rise of coke yield. These results suggested the dominative effect of strong acidic sites, that existed in the vicinity of Si-domains, on coking. As known in the foregoing acidity section, well-spread Si favored intermediate acidity and improved *iso*-butene selectivity, while deep dealumination destroyed zeolite structure (amorphous $AlPO_4$ was then formed) and led to a poor product distribution.

Table 2
Product distribution of linear butenes isomerization over No. 1-L1 SAPO-11 sample (wt.%)

Product	Reaction temperature (K)			
	613	673	773	823
C_3 and lighter hydrocarbon	0.26	0.42	0.84	1.97
Butane	35.19	37.31	39.34	40.23
iso-Butene	1.41	6.45	16.74	16.64
Linear butenes	63.10	55.70	42.64	39.17
C_5 and heavier hydrocarbon	0.04	0.10	0.30	0.84
Coke	0	0.02	0.14	1.15

3.3. Toluene catalytic disproportionation

Toluene disproportionation in existence of Mordernite and ZSM-5 zeolites was commercially used for production of xylene, especially

Table 3
Product distribution of toluene disproportionation over No. 1-L1 SAPO-11 sample (wt.%)

Product	Reaction temperature (K)			
	753	773	783	803
Non-aromatic hydrocarbon	0	0.01	0.03	0.09
Benzene	1.37	1.85	2.44	3.29
Toluene	96.20	95.70	94.40	92.60
p-Xylene	0.37	0.456	0.58	0.67
m-, *o*-Xylene	1.46	1.98	2.57	3.38

Table 4
Product distribution of cumene cracking over No. 1-L1 SAPO-11 sample (wt.%)

Product	Reaction temperature (K)			
	653	673	683	703
C_{1-2}	0.18	0.40	0.66	1.37
C_3	2.78	3.81	4.77	5.99
C_{4-6}	0.09	0.18	0.35	0.77
Benzene	4.62	6.72	8.94	12.84
Cumene	92.30	88.80	85.10	78.60
Coke	0.03	0.09	0.18	0.43

p-xylene, and was still gaining more attentions in laboratory studies [19–21]. SAPOs molecular sieves due to their unique acidic properties were recently applied for toluene disproportionation [22]. In this paper, SAPO-11 molecular sieve was tested by toluene disproportionation. Table 3 exemplified the results of toluene disproportionation on No. 1-L1 SAPO-11 sample. The reaction products contained benzene, xylene, methane, ethane and ethene. The non-aromatic hydrocarbons were from side reactions such as dealkylation of aromatics, oligomerization of carbenium and cracking of the oligomers. Coke was not detected due to the mild reaction conditions.

Disproportionation of short chain alkylbenzenes was mainly proceeded on Lewis sites via spillover of the short chain alkyl group and hydrogen proton [23,24]. Benzene ring was hardly changed under the evaluation conditions. Therefore, toluene disproportionation activity was expressed, based on benzene ring balance, by (molar yield of benzene and xylene minus molar yield of carbon atoms in non-aromatic hydrocarbons)/(molar yield of benzene, toluene and xylene). Side reaction selectivity was ex-

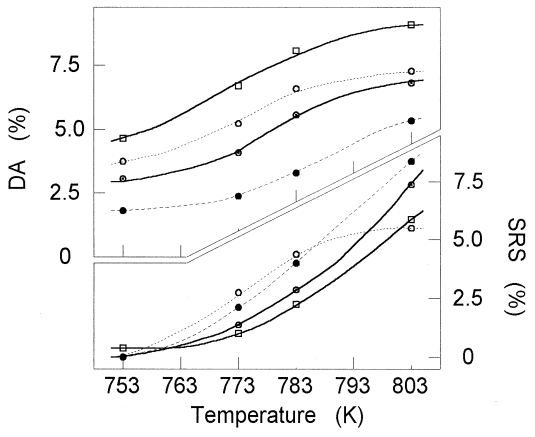

Fig. 5. Temperature dependence of toluene disproportionation activity (DA) and side reaction selectivity (SRS) over No. 1 SAPO-11 sample (· · · ○), No. 2 SAPO-11 sample (——— □), No. 1-L1 SAPO-11 sample (———⊙) and No. 1-L2 SAPO-11 sample (---●) in Table 1.

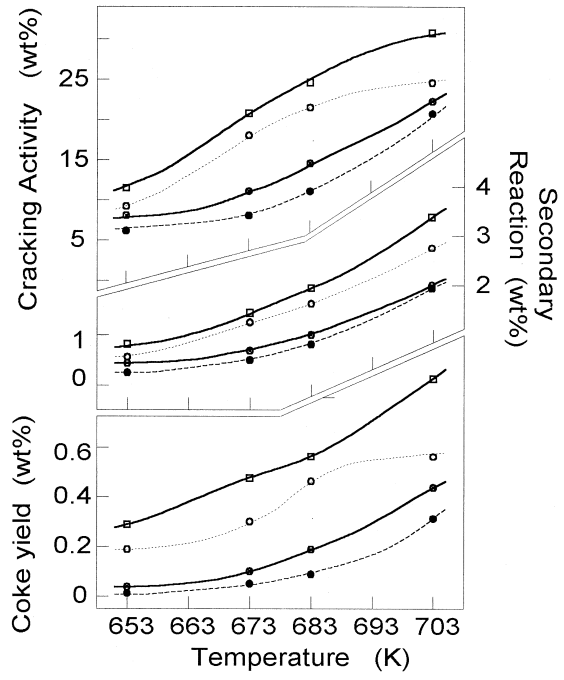

Fig. 6. Temperature dependence of cumene cracking activity, secondary reaction performance and coke yield over No. 1 SAPO-11 sample (· · · ○), No. 2 SAPO-11 sample (——— □), No. 1-L1 SAPO-11 sample (———⊙) and No. 1-L2 SAPO-11 sample (---●) in Table 1.

pressed by (molar yield of carbon atoms in non-aromatic hydrocarbons)/(molar yield of benzene and xylene). Fig. 5 presents the toluene disproportionation activity and side reaction selectivity of SAPO-11 samples at different temperatures. Toluene diaproportionation increased with temperature. Dealuminated SAPO-11 samples had lower toluene disproportionation activity than the initial SAPO-11 sample due to destroy of acidic sites by dealumination. It was noted that side reactions increased with temperature in a larger speed than the disproportionation reaction, and the former was more sensitive to temperature than the later. To increase xylene yield, therefore, reaction should performed at lower temperature and space velocity.

3.4. Cumene catalytic cracking

Cumene cracking has been used as a test for acid sites on amorphous aluminum silicate catalysts for decades [25]. Strong acidity especially Bronsted sites favored cumene cracking [26]. The cracking products contained benzene, propene and other non-aromatic hydrocarbons. Table 4 lists an example of cumene cracking on SAPO-11 molecular sieve (No. 1-L1 sample) at variant temperatures. Differently from toluene disproportionation (Table 3), it was observed an evident coking phenomenon during cumene cracking. Therefore, oligomerization of cracking product such as propyl cation was severe on SAPO-11 molecular sieve during cumene cracking.

Fig. 6 depicts temperature dependence of cumene cracking activity, coke yield and secondary reaction behavior of cracking products. Cumene cracking activity was expressed by (100 minus weight percentage of unreacted cumene in product). Secondary reactions envolved oligomerization of cracking products and decomposition of the oligomers, and were measured by weight percentage yield of C_{1-2} and C_{4-6}. It was noted that, within the evaluation

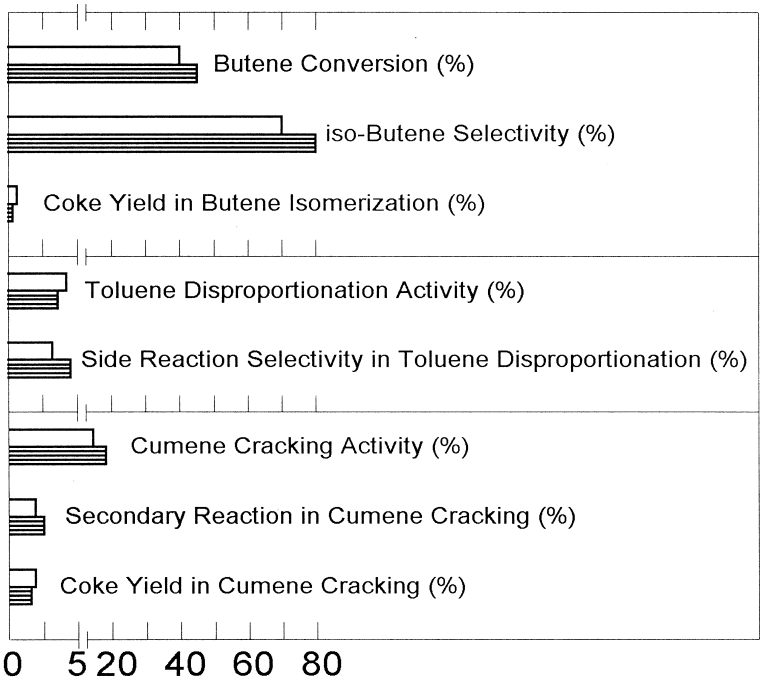

Fig. 7. Influence of trace amount of water on catalytic behavior of No. 1-L1 SAPO-11 sample (shadow bar). Black bar is the case before water was introduced. Reaction temperature was 673, 783 and 683 K for butene isomerization, toluene disproportionation and cumene cracking, respectively.

temperature range, fresh SAPO-11 samples (No. 1 and No. 2 samples in Table 1) showed higher cracking activity, coke yield and secondary reaction rate than dealuminated samples (No. 1-L1 and No. 1-L2 samples in Table 1). Since strong acidic sites were formed in dealuminated samples, cracking activity and coke yield increased with temperature more quickly than that of the fresh samples. No. 2 SAPO-11 sample possessed large acidity due to high Si content and showed significant cracking and coking activity, even though it was not dealuminated. Therefore, strong acidity favored both cumene cracking and coking reactions.

3.5. Influence of trace amount of water on catalytic behavior

Trace amount of H_2O vapor was introduced into reaction system from a saturator during activity evaluation for No. 1-L1 SAPO-11 sample. This affected the catalytic performance in a great deal as shown in Fig. 7. Chemisorption of water vapor modified surface acidity of the SAPO-11 sample by conversing Lewis sites into Bronsted sites. The intermediate acidity increased due to occurrence of the novel Bronsted sites, that enhanced both butene isomerization and cumene cracking. The reduce of Lewis sites, especially strong acidic sites, inhibited the coking tendency in butene isomerization and cumene cracking. Toluene disproportionation was moderated by H_2O chemisorption, while side reactions such as dealkylation of toluene, oligomerization of methyl cation and cracking of the oligomers in toluene conversion increased.

4. Conclusion

Si domains were formed in SAPO-11 when synthesis mixture contained excessive Si. During dealumination, Al adjacent to Si in SAPO-11 was firstly removed, that led to formation of Si domains, and amorphous $AlPO_4$ was then resulted.

SAPO-11 possessed intermediate acidity. Si domains induced strong acidic sites, and amorphous $AlPO_4$ destroyed the acidity distribution. Dealumination reduced catalytic activity of SAPO-11 samples for butene isomerization and toluene disproportionation. Dealuminated samples had severe coking yield. Cumene cracking on dealuminated SAPO-11 samples was more sensitive to temperature than that on fresh samples. Adjustment of the acidity of SAPO-11, by introducing trace amount of water vapor into reaction system, favored *iso*-butene formation and cumene cracking, while coking phenomenon and toluene disproportionation were inhibited.

Acknowledgements

The authors thank Ms. Hao for preparing the manuscript and SINOPEC for financial support. The authors also gratefully acknowledge the anonymous referees for the constructive suggestion, and English grammar correction.

References

[1] M.J.G. Janssen, W.J. Mortier, C.W.M. Van Oorschot, M. Makkee, WO 9118851, 1991.
[2] J. Houzvicka, V. Ponec, Catal. Rev. Sci. Eng. 39 (1997) 319.
[3] C.W. Lee, G. Brouet, X. Chen, L. Keven, Zeolites 13 (1993) 565.
[4] S.M. Yang, K.J. Wang, Stud. Surf. Sci. Catal. 97 (1995) 453.
[5] S. Subramanian, A. Mitra, C.V.V. Satyanarayana, D.K. Chakrabarty, Appl. Catal. 159 (1997) 229.
[6] T. Matsuda, T. Kimura, E. Herawati, C. Kobayashi, E. Kikuchi, Appl. Catal. 136 (1996) 19.
[7] J.A. Martens, B. Verlinden, M. Merlens, P.J. Grobet, P.A. Jacobs, ACS Symposium Series 398 (1989) 305.
[8] B.M. Lok, C.A. Messina, R.L. Patton, R.T. Gajek, T.R. Cannan, E.M. Flanigen, US Patent 4440871, 1984.
[9] H. Tian, C. Li, Stud. Surf. Sci. Catal. 105 (1997) 1397.
[10] R. Khouzami, G. Coudurier, F. Lefebvre, J.C. Vedrine, B.F. Mentzen, Zeolites 10 (1990) 183.
[11] J.A. Martens, P.J. Grobet, P.A. Jacobs, J. Catal. 126 (1990) 299.
[12] J.C. Vedrine, Stud. Surf. Sci. Catal. 69 (1991) 15.

[13] M. Derewinski, M.J. Peltre, M. Briend, D. Barthomeuf, P.P. Man, J. Chem. Doc. Faraday Trans. 89 (1993) 1823.
[14] D. Barthomeuf, Zeolites 14 (1994) 194.
[15] Q.H. Xu, A.Z. Yan, S.L. Bao, K.J. Xu, Stud. Surf. Sci. Catal. 28 (1986) 835.
[16] J.A. Martens, P.A. Jacobs, Stud. Surf. Sci. Catal. 85 (1994) 653.
[17] V. Zholobenko, A. Garforth, L. Clark, J. Dwyer, Stud. Surf. Sci. Catal. 97 (1995) 359.
[18] A.C. Butler, C.P. Nicolaides, Catal. Today 18 (1993) 443.
[19] K.P. Kelly, J.R. Butler, Eur. Pat. Appl. EP 819666, 1998.
[20] M. Paciga, A. Smieskova, P. Huder, Z. Zidek, React. Kinet. Catal. Lett. 60 (1997) 21.
[21] J.S. Beck, T.F. Kinn, S.B. McCullen, D.H. Olson, US 5659098, 1997.
[22] L.N. Radev, V.J. Penchev, React. Kinet. Catal. Lett. 58 (1996) 139.
[23] H. Tian, ACS Book Series, accepted.
[24] J. Meusinger, H. Vinek, G. Dworeckow, M. Goepper, J.A. Lercher, Stud. Surf. Sci. Catal. 69 (1991) 373.
[25] J.W. Ward, J. Catal. 9 (1967) 225.
[26] M. Ziolek, I. Nowak, Catal. Lett. 45 (1997) 259.